Effects of Nonplanar Outboard Wing Forms on a Wing

D. A. Naik*
ViGYAN, Inc., Hampton, Virginia
and
C. Ostowari†
Texas A&M University, College Station, Texas

It is possible for a constant span to obtain better aerodynamic performance from a wing with a nonplanar outboard wing form than from a wing with a planar outboard form, despite the added drag from the increased wetted area. Furthermore, the semispan rolling-moment characteristics indicate the lower wing-root bending moment for some nonplanar configurations. These conclusions are based on an experimental and computational investigation of the aerodynamic characteristics of planar and nonplanar outboard wing forms. Seven different configurations—planar rectangular, nonplanar rising arc, nonplanar drooping arc, planar sheared, sheared with dihedral, sheared with anhedral, and planar elliptical—were investigated for two different spans. Flow-visualization photographs indicate that there are three vortex systems associated with the sheared forms. The lower induced drag coefficients of nonplanar wings are believed to accrue from the movement of vorticity away from the center-of-span line, resulting, in some instances, in induced efficiencies higher than that of a planar elliptical wing. Flow surveys indicate that the effective span, as determined by the location of the tip vortex, might not be a sufficient yardstick of the induced performance of a nonplanar wing.

Nomenclature

$\mathcal{R}$ = aspect ratio, = b^2/S
b = span
c = reference chord
C_D = drag coefficient, = drag/qs
C_l = rolling- (or root-bending) moment coefficient, = moment/qSb
C_L = lift coefficient, = lift/qS
$C_L\alpha$ = lift slope per degree
C_m = pitching-moment coefficient, = moment/qSc
e = induced (or span) efficiency factor
K = profile drag magnification factor
q = freestream dynamic pressure
RN = Reynolds number, wrt c
S = planform area
α = angle of attack

Subscripts
s = stall
0 = zero-lift condition

Introduction

FOR a subsonic airplane, induced drag comprises roughly one-third of the total drag in cruise and roughly one-half of the total drag in climb. Traditionally, for a given span, the twist and planform of the wing are designed for optimal induced performance.

Some research has concentrated on in-plane planform modifications alone. For instance, Weihs and Ashenberg[1] showed that the minimum induced drag of a flat elliptical wing can be obtained "with planforms of both forward and rearward sweep and curvature." Van Dam[2] observed that, in nature, various cruising fish and birds have crescent-shaped tails of moderate-to-high aspect ratio. He used VSAERO[3,4] to "demonstrate that an untwisted planar crescent-moon wing can be more efficient than an unswept elliptical wing." Vijgen et al.[5] showed that sheared (swept and tapered) planar wingtips could improve aerodynamic efficiency.

This paper describes an investigation of further improving induced performance by means of nonplanar wing forms. Pertinent research is discussed here; a more comprehensive discussion of related work is available elsewhere.[6] Cone[7] used a variation of the lifting line, called the lifting arc, to show that "many nonplanar wing forms exist which are more efficient, from the induced drag standpoint, than optimum flat wings with greater spans." As modern fabrication techniques and the use of composite materials have resulted in significant advances in wing weight reduction, nonplanar wing forms merit renewed consideration.

Cone calculated that it is possible to get span efficiency factors of greater than 1, even up to 1.5, with either nonplanar tip modifications or nonplanar total-span modifications. "Some tip alterations can result in far greater efficiency increases than those produced by radical modification of the entire span." Basically, the greatest increases in span efficiency occur for "modifications which tend to release the major portion of vorticity near the tip and over an appreciable vertical area."

This paper shows the effects of various nonplanar outboard wing forms, circular arcs, and also sheared forms with dihedral or anhedral. The planar counterparts to these forms and a compromise elliptical outboard planform, are included for comparison. The induced efficiency is used as an index of wing-form performance. Other important factors are the total drag (as pressure and skin-friction drag change with wetted area), the wing-root bending moment (a measure of the structural requirements[8]), and the tip vortex location (a measure of the effective span). The relatively elementary forms used in this work are intended merely to illustrate trends. They are not intended to represent practical designs.

Model Description and Procedure

When comparing the induced efficiencies of different wing forms, it is more appropriate to keep the model spans constant, instead of keeping the aspect ratio constant. The model

Presented in part as Paper 88-4.3.2 at the 16th International Council of Aeronautical Sciences Congress, Jerusalem, Israel, Aug. 28–Sept. 2, 1988; received Sept. 29, 1988; revision received May 15, 1989.

*Research Engineer. Member AIAA.
†Associate Professor, Aerospace Engineering Department. Member AIAA.

wing forms are sketched in Fig. 1. Pertinent dimensions and aspect ratios are given in Table 1. The aspect ratios are defined with respect to the projected area.[7]

An untwisted, untapered, unswept, rectangular wing with no dihedral was used as the inboard wing form. The airfoil was a 15%-thick symmetrical section. This section, designated WSU 0015,[9] was designed using the Eppler code.[10] The chord was 1 ft (0.3048 m). The model was of the reflection plane type with the base mount in the tunnel floor. The tip edge was flat. An inboard portion, 1.5 ft (0.4572 m), of this wing could be removed to provide the smaller reference span. Furthermore, the outboard 0.75 ft (0.2286 m) of this wing could be removed and replaced with the wing forms described subsequently.

The sheared outboard planform had a projected length of 0.75 ft (0.2286 m), root chord of 1 ft (0.3048 m), a tip chord of 0.25 ft (0.0762 m), and a sweepback of 60 deg. A removable fillet could be inserted to provide this planform with a 45-deg dihedral or anhedral while keeping the overall model span constant. Another outboard planform used in this study was a constant-chord circular arc of radius 0.75 ft (0.2286 m). Depending on the orientation of the wind vector, this could be viewed as either a rising- or drooping-arc outboard planform. The elliptical outboard planform had semiminor and semimajor axes of length of 0.5 ft (0.1524 m) and 0.75 ft (0.2286 m), respectively.

The experiments were conducted at the Texas A&M University 7- × 10-ft (2.13- × 3.05-m) low-speed wind tunnel. The tunnel has a turbulence factor of 1.1. Relevant measurement resolutions are given in Table 2.

A chord RN of 1.3×10^6 was used for the tests. The dynamic pressure needed to achieve this RN was 49 psf (2.35×10^3 Pa). The freestream windspeed was about 203 ft/s (62 m/s). The corresponding Mach number is roughly 0.18. The angle-of-attack range studied was −4 to 20 deg, in increments of 2 deg in the linear lift region and 1 deg in the nonlinear range. Boundary-layer trip strips were used to fix the transition location at 0.05 c upper surface and 0.05 c lower surface.

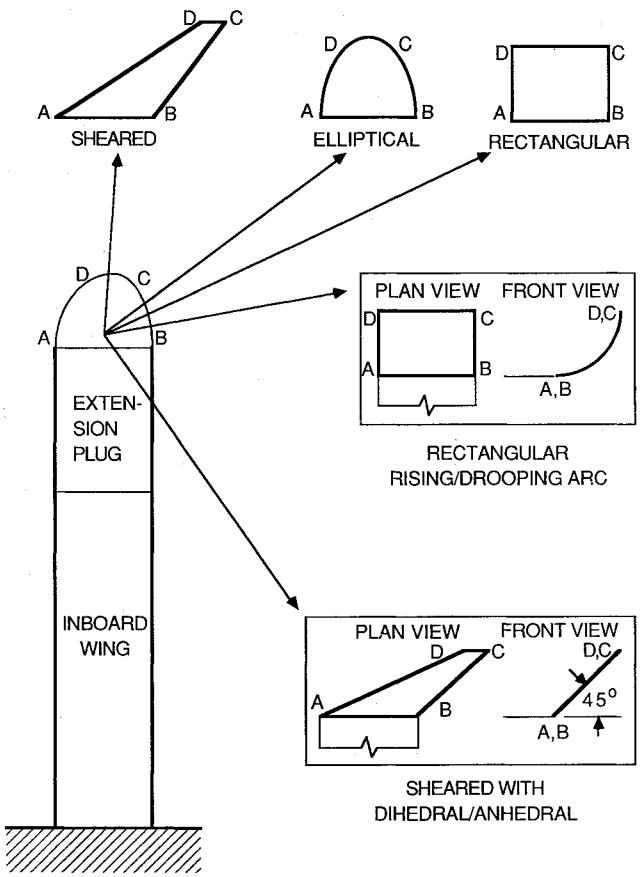

Fig. 1 Sketch of model configurations.

The forces and moments were resolved with respect to the quarter-chord location on the root section. The measured data were corrected following the standard procedure given by Rae and Pope.[11] The drag data were also corrected for the drag of the trip strips.[11] The fluorescent oil-flow technique was employed for the surface flow-visualization studies.

The location of the tip vortex, as indicated by the crossflow velocities, was obtained from three-dimensional, hot-film, constant-temperature anemometer surveys of the flowfield. A planar survey grid perpendicular to the freestream velocity was studied at the 0.2 c downstream location aft of the tip trailing edge. At this location, the vortex core is expected to have developed sufficiently to be distinguishable from the rest of the flow.[12] Because of the probe volume, the grid mesh could not be finer than 0.25 in. (6.35 mm). A nonnulling seven-hole probe was then used to obtain more accurate information of the vortex velocities and pressures.

In addition to the experiments, these models were analyzed with VSAERO.

Results

Rising and Drooping Wing Forms

Force and moment coefficient experimental data for the smaller span rectangular wing forms are given in Fig. 2. The data, along with the data for the longer span, are summarized in Table 3. The rising arc has higher lift-curve slope than its planar counterpart, Fig. 2a.

The higher zero-lift drag coefficient of the nonplanar wings arises from the added wetted area. The drag polars shown in Fig. 2b are restricted primarily to the linear lift range for clarity. The drooping wing has lower total drag than the planar wing beyond a C_L of 0.38. For the rising arc, this crossover occurs at a C_L of 0.8. The better induced performance of the nonplanar wings, particularly of the drooping arc, is shown more clearly in the incremental drag ($C_D - C_{D\min}$) plots of Fig. 2c. This induced performance is quantified in terms of the induced efficiency, which is calculated from[6,13]

$$C_D = C_{D\min} + C_L^2/\pi \mathcal{A} e \tag{1}$$

The induced efficiencies shown in Table 3 are calculated using the experimental data (e_{expt}) and also using results from the panel method (e_{VSAERO}). The definition does not include the profile drag variation with lift coefficient, which is typically

Table 1 Model aspect ratios

Semispan	1.68 m	1.22 m
	Planar[a]	
Rectangular	11.000	8.000
Elliptical	11.332	8.335
Sheared[b,c]	11.593	8.605
	Nonplanar[a]	
Sheared + dihedral[b-d]	11.413	8.419
Sheared + anhedral[b-d]	11.413	8.419
Rising arc	11.000	8.000
Drooping arc	11.000	8.000

[a]Outboard planform projected length = 0.2286 m (0.75 ft). [b]Sweep = 60 deg. [c]Taper ratio = 0.25. [d]Dihedral/anhedral = 45 deg.

Table 2 Measurement resolution

Quantity	Resolution[a]
C_D	±0.00015
C_L	±0.002
C_l	±0.0015
C_m	±0.0005

[a]These are the upper limits. Expected uncertainties will be lower.

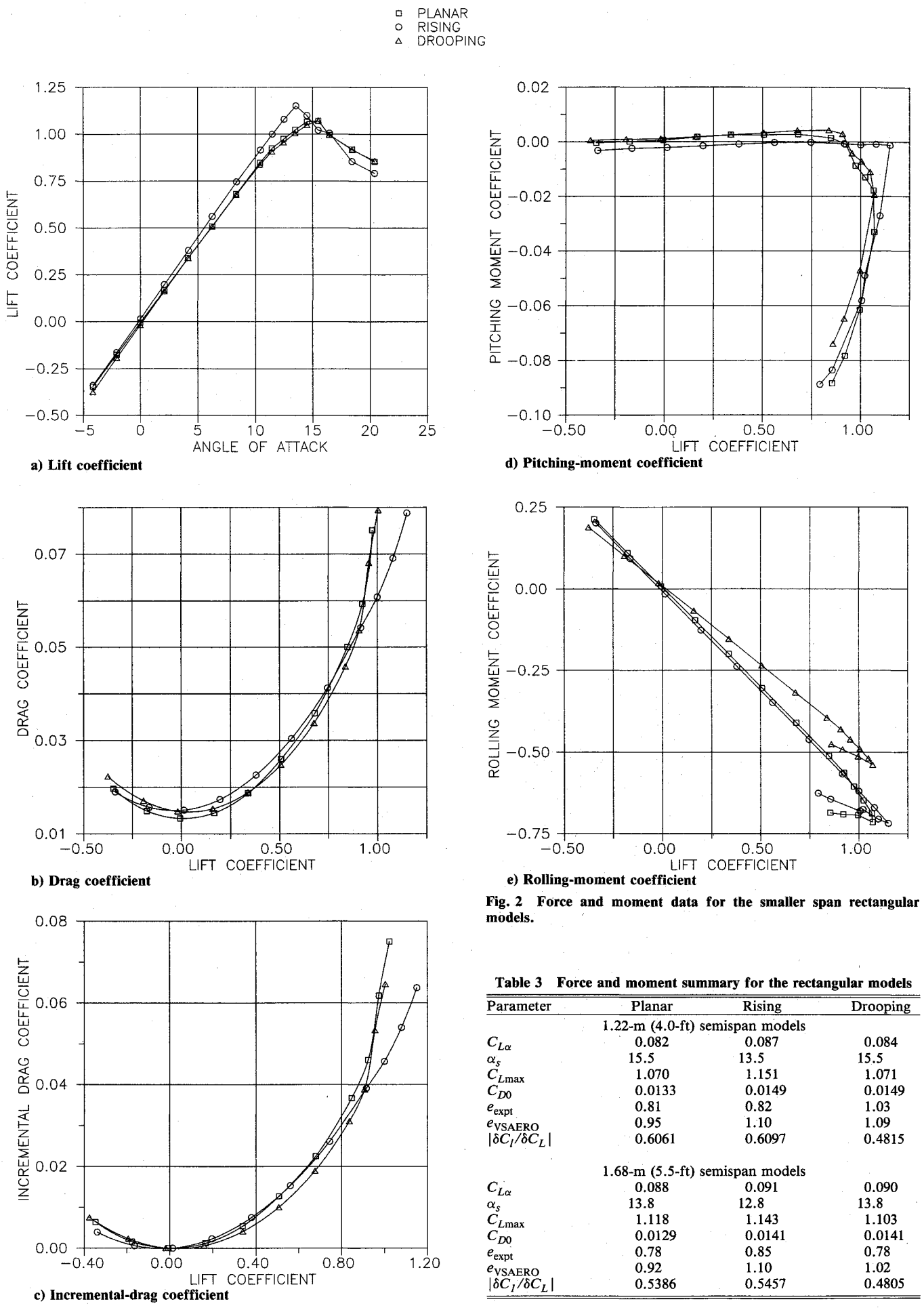

a) Lift coefficient

b) Drag coefficient

c) Incremental-drag coefficient

d) Pitching-moment coefficient

e) Rolling-moment coefficient

Fig. 2 Force and moment data for the smaller span rectangular models.

Table 3 Force and moment summary for the rectangular models

Parameter	Planar	Rising	Drooping
	1.22-m (4.0-ft) semispan models		
$C_{L\alpha}$	0.082	0.087	0.084
α_s	15.5	13.5	15.5
$C_{L\max}$	1.070	1.151	1.071
C_{D0}	0.0133	0.0149	0.0149
e_{expt}	0.81	0.82	1.03
e_{VSAERO}	0.95	1.10	1.09
$\lvert\delta C_l/\delta C_L\rvert$	0.6061	0.6097	0.4815
	1.68-m (5.5-ft) semispan models		
$C_{L\alpha}$	0.088	0.091	0.090
α_s	13.8	12.8	13.8
$C_{L\max}$	1.118	1.143	1.103
C_{D0}	0.0129	0.0141	0.0141
e_{expt}	0.78	0.85	0.78
e_{VSAERO}	0.92	1.10	1.02
$\lvert\delta C_l/\delta C_L\rvert$	0.5386	0.5457	0.4805

quadratic in nature. Thus, a reasonable modification to the equation would be

$$C_D = C_{D\min} + C_L^2[K + 1/\pi \mathcal{A}e] \quad (2)$$

where K is the profile drag magnification factor. Aerodynamic calculations from a panel method were then used in conjunction with the experimental data to estimate K. A typical value of K was found to be 0.007. The actual efficiency of a particular wing will be between e_{VSAERO} (the upper bound) and e_{expt} (the lower bound). The e_{expt} for the smaller drooping wing shows that the actual e for this wing is, in any event, greater than 1.

Spanwise circulation distributions for the smaller span models, calculated using VSAERO, are shown in Fig. 3. (The symbols in Fig. 3 are used merely to facilitate comparison with Fig. 2; they do not represent experimental data.) These distributions correspond to an angle of attack of 8 deg. For each wing, the "outboard" portion of the planform starts just beyond the 0.80 spanwise station. The distributions are also the spanwise load distributions, because all three configurations are of constant chord. The drooping curve has loading comparable to the planar. The rising curve has noticeably higher loading throughout.

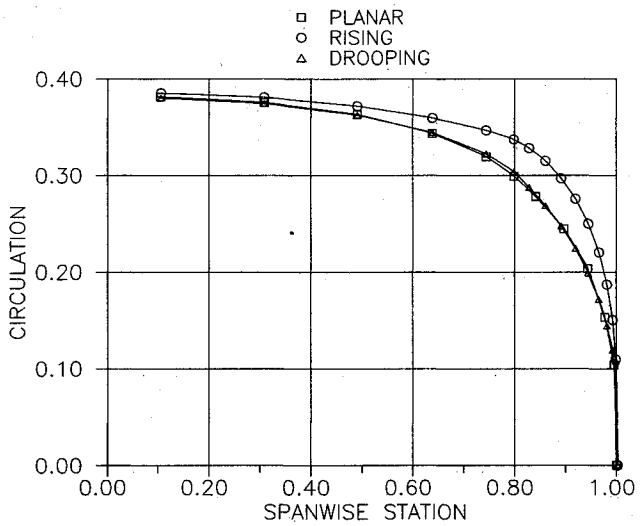

Fig. 3 VSAERO-derived circulation distributions for the smaller span rectangular models at $\alpha = 8$ deg.

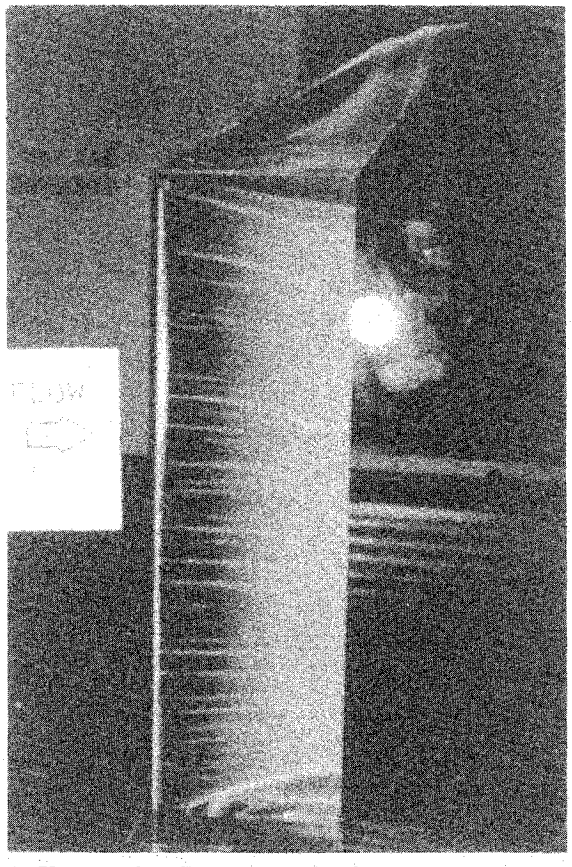

Fig. 4 Upper surface flow visualization for the smaller span planar sheared model at $\alpha = 12$ deg.

The pitching-moment curves for the rising and drooping arcs are relatively flat in the linear lift range, Fig. 2d. The primary contributor to the root bending moment (or semispan rolling moment, Fig. 2e) is the lift force. In addition, a side force generated by the nonplanar portion of the planform increases gradually with angle of attack and, as a consequence, contributes to the root bending moment through a small moment arm. With the onset of flow separation, the spanwise location of the center of lift changes erratically with changing angle of attack. Hence, the relationship between bending moment and lift is no longer linear. The slopes of the linear portion of the rolling-moment characteristics are given in Table 3. The drooping wing has the lowest rolling-moment coefficient for positive lift coefficient. This implies a bending-moment advantage in terms of lower material strength requirements than either the planar or the rising arc.

In summary: even if one discounts the theoretical efficiencies, circulation distributions, and induced drags, the experimental force data alone show that the drooping-arc nonplanar wing has aerodynamic advantages when compared to its planar counterpart. The drawback is the larger zero-lift drag coefficient because of the larger wetted area. However, this nonplanar wing has lower total drag for a large portion of the linear lift range, Fig. 2b.

Sheared Forms with Dihedral/Anhedral

The nonplanar sheared forms at 45-deg anhedral or dihedral do not seem to offer any aerodynamic advantages—other than lower bending moment—over their planar sheared counterpart, Table 4. However, a VSAERO-based parametric study of nonplanar sheared outboard planforms with varying dihedral/anhedral demonstrated that, for greater than 45-deg dihedral/anhedral, both induced drag and root bending-moment benefits might be achieved with the nonplanar forms.[6]

Planar Wing Forms

Although the three planar forms are quite different from a geometrical standpoint, their gross aerodynamic characteristics are closely allied, Table 5. The sheared has the best overall performance, but only marginally.

The surface flow visualization for the sheared planform, Fig. 4, suggests that there are three vortex systems in effect near the outboard wing simultaneously: a tip vortex, a separation-induced leading-edge vortex, and a secondary

Table 4 Force and moment summary for the sheared models

Parameter	Planar	Dihedral	Anhedral
	1.22-m (4.0-ft) semispan models		
$C_{L\alpha}$	0.084	0.081	0.079
α_s	15.5	14.5	15.4
$C_{L\max}$	1.098	1.118	1.025
C_{D0}	0.0127	0.0128	0.0128
e_{expt}	0.79	0.71	0.83
e_{VSAERO}	0.99	0.98	0.94
$\lvert\delta C_l/\delta C_L\rvert$	0.6000	0.5881	0.4454
	1.68-m (5.5-ft) semispan models		
$C_{L\alpha}$	0.090	0.088	0.085
α_s	13.8	12.8	14.8
$C_{L\max}$	1.129	1.086	1.107
C_{D0}	0.0125	0.0126	0.0126
e_{expt}	0.78	0.68	0.80
e_{VSAERO}	0.98	0.98	0.94
$\lvert\delta C_l/\delta C_L\rvert$	0.5288	0.5226	0.4526

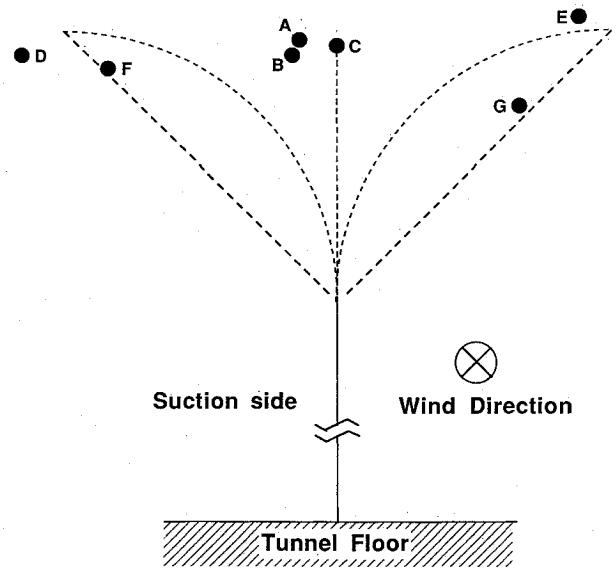

Fig. 5 Vortex positions from Table 6 for the smaller span models at $\alpha = 8$ deg.

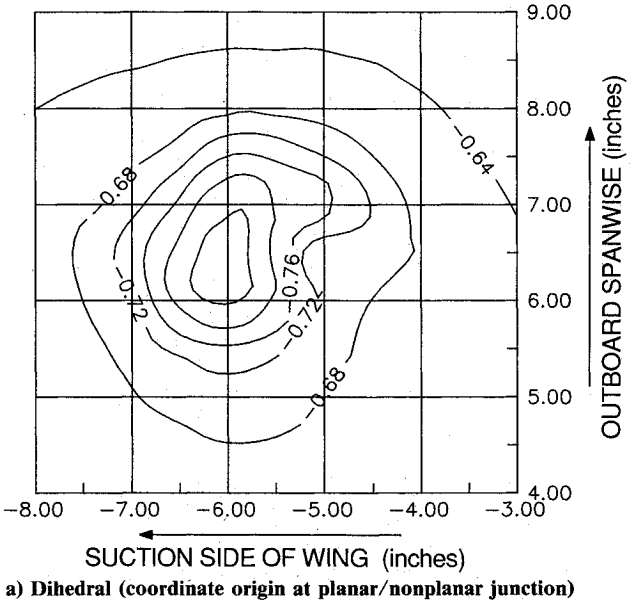

a) Dihedral (coordinate origin at planar/nonplanar junction)

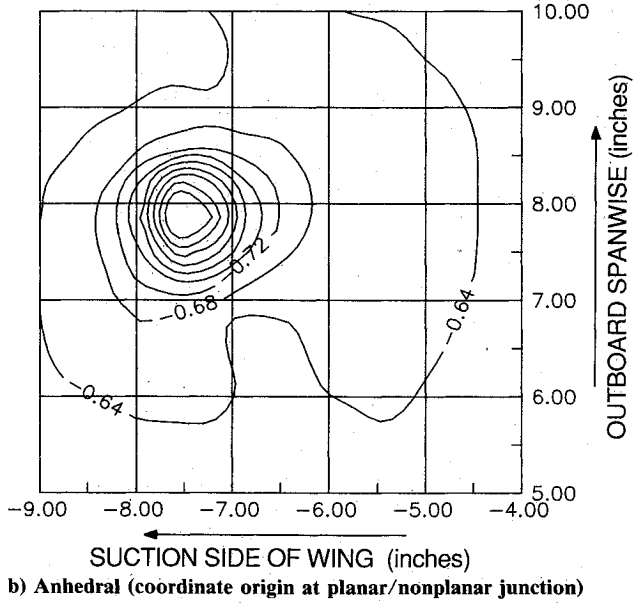

b) Anhedral (coordinate origin at planar/nonplanar junction)

Fig. 6 Vortex static pressure contours for the smaller span nonplanar sheared models at $\alpha = 8$ deg.

Table 5 Force and moment summary for the planar models

Parameter	Rectangular	Elliptical	Sheared
	1.22-m (4.0-ft) semispan models		
$C_{L\alpha}$	0.082	0.082	0.084
α_s	15.5	15.5	15.5
$C_{L\max}$	1.070	1.104	1.098
C_{D0}	0.0133	0.0128	0.0127
e_{expt}	0.81	0.82	0.79
e_{VSAERO}	0.95	0.96	0.99
$\lvert\delta C_l/\delta C_L\rvert$	0.6061	0.6018	0.6000
	1.68-m (5.5-ft) semispan models		
$C_{L\alpha}$	0.088	0.088	0.090
α_s	13.8	13.8	13.8
$C_{L\max}$	1.118	1.118	1.129
C_{D0}	0.0129	0.0139	0.0125
e_{expt}	0.78	0.85	0.78
e_{VSAERO}	0.92	0.94	0.98
$\lvert\delta C_l/\delta C_L\rvert$	0.5386	0.5344	0.5288

Table 6 Vortex locations and approximate sizes

Model	Location[a]	Size[b]
A Rectangular	(0.10 c, 0.995 $b/2$)	$>0.3c$
B Elliptical	(0.13 c, 0.984 $b/2$)	$0.3c$
C Sheared	(0.00 c, 0.990 $b/2$)	$0.3c$
D Rising	(0.79 c, 0.984 $b/2$)	$0.3c$
E Drooping	(0.67 c, 1.010 $b/2$)	$0.2c$
F Dihedral	(0.63 c, 0.974 $b/2$)	$0.3c$
G Anhedral	(0.50 c, 0.948 $b/2$)	$0.2c$

[a]These locations are sketched in Fig. 5. Abcissas are wrt the inboard model plane. Ordinates are wrt the tunnel floor. All coordinates are absolute values. [b]The "size" is the average diameter of the -0.68 static pressure contour.

vortex that sheds from the junction of the inboard rectangular planform with the outboard sheared planform.

Flow Surveys

Only the tip vortices were surveyed. For largely unseparated conditions, i.e., the linear lift range, the vortex is not expected to shift appreciably.[12] This finding was confirmed here for surveys conducted at 8-, 10-, and 12-deg angles of attack. Thus, it is not improper to compare the vortex locations of different configurations at the same angle of attack.

The vortex locations for the smaller span models are given in Table 6. The locations are accurate to 0.125 in. (3 mm). The location ordinates are also the effective semispan. This use of the vortex location just aft of the trailing edge to estimate effective span is consistent with the work of others. Hoerner[14] shows evidence that the widest effective spans "are generally the ones exhibiting the least drag due to lift." For convenience, the vortex locations, given in Table 6, are sketched in Fig. 5.

For all three planar models, the tip vortex is within an inch (2.54 cm) inboard of the tip edge. However, the vortex for the sheared planform is closest to the wing upper surface. These differences apparently have minimal effect on the overall aerodynamic characteristics of the planar configurations.

The vortex for the rising arc (D in Fig. 5) is located roughly 0.75 in. (19 mm) inboard of the wingtip. This spanwise location is comparable to the location for the three planar forms. However, the vortex is 0.8 c above the inboard wing plane. For the drooping arc, the vortex (E in Fig. 5) is roughly 0.50 in. (13 mm) outboard of the wingtip and is 0.67 c below the inboard wing upper surface.

The dihedral model has a vortex (F in Fig. 5) that is more outboard than that of the anhedral model (G in Fig. 5) at the same angle of attack. The dihedral has a larger effective span but, as seen in Table 4, not necessarily a higher efficiency.

Rough quantitative estimates of the size of the tip vortices were made by measuring the extent (average "diameters" as the contours are not circular) for an arbitrarily chosen (-0.68 for the sizes in Table 6) static pressure coefficient. Static and total pressure coefficients were obtained by nondimensionalizing the local pressure differences from the freestream conditions wrt the freestream dynamic pressure.

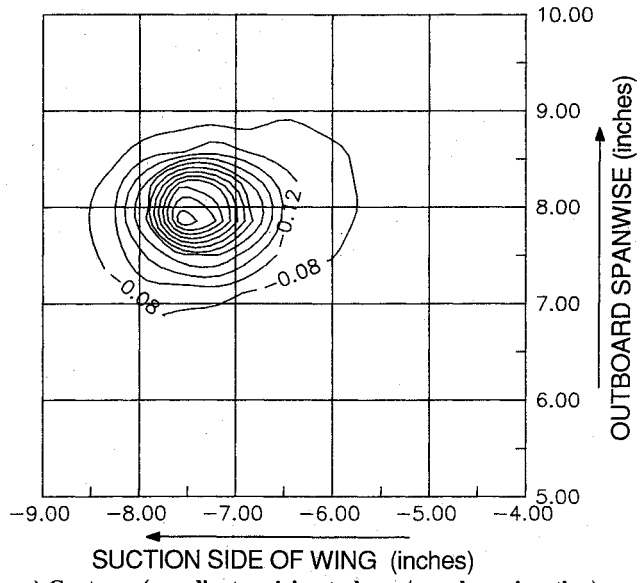

a) Contours (coordinate origin at planar/nonplanar junction)

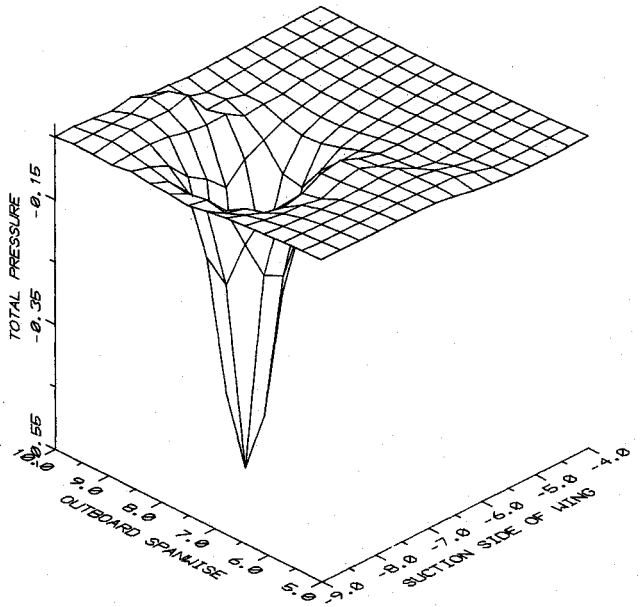

b) Surface (coordinate origin at planar/nonplanar junction)

Fig. 7 Vortex total pressure distributions for the smaller span anhedral model at $\alpha = 8$ deg.

The static pressure coefficient is expected to be zero at locations corresponding to the freestream conditions. It decreases as one progresses toward the vortex core. Inside the core, this coefficient is expected to reach a plateau at some negative value because of viscous effects.[15] This trend is seen in the contours for the dihedral (Fig. 6a) and anhedral (Fig. 6b).

Total pressure is expected to be constant in the outer inviscid portion of the vortex. In the core, the action of viscous forces causes a decrease in fluid mechanical energy that is reflected in the decrease in total pressure. The total pressure distribution for the anhedral wing at 8-deg angle of attack is shown both in the form of contours (Fig. 7a) and in the form of a three-dimensional view (Fig. 7b).

The outermost contour corresponds to a total pressure coefficient of -0.04. The inner contours have gradually increasing (in a negative sense) total pressure coefficients. This, again, is in agreement with expectations.[15] The three-dimensional view clearly shows the vortex core. There is a region of slightly positive total pressure just outside the vortex core. This apparent anomaly has been observed by other users of a seven-hole probe.[15]

The marginal differences in effective span between the nonplanar arcs and their planar counterpart indicate that a physically wider effective span, as defined here and in Ref. 14, is not the only means of improving efficiency. Rather, a strategic placement of the tip vortex and the resulting effect on the downwash distribution are the keys of improving span efficiency. Surveys further downstream (at points where most of the vorticity shed from the wing would be contained within the tip vortices) might shed more light on the relationship between effective span and induced efficiency.

Conclusions

This study demonstrates that, for a constant span, it is possible to obtain better induced efficiency with a nonplanar wing than from its planar counterpart. In some cases, the advantage is sufficiently favorable to overcome the skin-friction drag penalty from the larger wetted areas. Furthermore, in some instances, it is possible to achieve the aerodynamic improvement without a bending-moment penalty.

The lower induced drag coefficients of wings with nonplanar outboard planforms are believed to accrue from the movement of vorticity away from the center-of-span line. The study of the tip vortex location indicates that the effective span alone, as determined by the tip vortex, might not be a sufficient yardstick for the induced performance of a nonplanar wing. Rather, both the position of the vortex and its effect on the wing's downwash distribution are critical.

Acknowledgments

This work was supported by NASA Langley Research Center. Additional funding was provided by the Aerospace Engineering Department, Texas A&M University.

References

[1]Weihs, D. and Ashenberg, J., "Minimum Induced Drag of Wings with Curved Planform," *Journal of Aircraft,* Vol. 21, Jan. 1984, pp. 89–91.

[2]van Dam, C. P., "Induced-Drag Characteristics of Crescent-Moon-Shaped Wings," *Journal of Aircraft,* Vol. 24, Feb. 1987, 115–119.

[3]Maskew, B., "Prediction of Subsonic Aerodynamic Characteristics: A Case for Low-Order Panel Methods," *Journal of Aircraft,* Vol. 19, Feb. 1982, pp. 157–163.

[4]Maskew, B., "PROGRAM 'VSAERO'–A Computer Program for Calculating the Non-Linear Aerodynamic Characteristics of Arbitrary Configurations," NASA CR-166476, Dec. 1982.

[5]Vijgen, P. M. H. W., van Dam, C. P., and Holmes, B. J., "Sheared Wing-Tip Aerodynamics: Wind-Tunnel and Computational Investigation," *Journal of Aircraft,* Vol. 26, March 1989, pp. 207–213.

[6]Naik, D. A. and Ostowari, C., "Experimental Investigation of Non-Planar Sheared Outboard Wing Planforms," AIAA Paper 88-2549, June 1988.

[7]Cone, C. D. Jr., "The Theory of Induced Lift and Minimum Induced Drag of Nonplanar Lifting Systems," NASA TR-R-139, 1962.

[8]Heyson, H. H., Riebe, G. D., and Fulton, C. L., "Theoretical Parametric Study of the Relative Advantages of Winglets and Wing-Tip Extensions," NASA TP-1020, Sept. 1977.

[9]Narramore, J. C., Wentz, W. H. Jr., and Ostowari, C., "Evaluation of a Procedure for the Design of Low-Speed Airfoils: Analytical and Experimental Results for a 15% Thick Symmetrical Section Airfoil with Control System," Wichita State Univ., Wichita, KS, Rept. AR-79-5, Oct. 1979.

[10]Eppler, R. and Sommers, D. M., "A Computer Program for the Design and Analysis of Low Speed Airfoils," NASA TM-80210, Aug. 1980.

[11]Rae, W. H. Jr. and Pope, A., *Low-Speed Wind Tunnel Testing,* 2nd ed., Wiley, New York, 1984.

[12]Francis, M. S. and Kennedy, D. A., "Formation of a Trailing Vortex," *Journal of Aircraft,* Vol. 16, March 1979, pp. 148–154.

[13]Anderson, J. D. Jr., *Introduction to Flight,* 2nd ed., McGraw-Hill, New York, 1985, pp. 213–221.

[14]Hoerner, S. F., *Fluid-Dynamic Drag,* published by the author, Brick Town, NJ, 1965, pp. 7-5–7-6.

[15]Reed, L., Mattingly, J. D., and Jonas, F. M., "The Seven-Hole Pressure Probe," USAF Academy, CO, Rept. USAFA-TN-84-9, 1984.